Electronic properties of twisted multilayer graphene

IOP Publishing J. Phys. Mater. 5 (2022) 034003 https://doi.org/10.1088/2515-7639/ac6c4a

Journal of Physics: Materials

OPEN ACCESS

RECEIVED
16 March 2022

REVISED
29 April 2022

ACCEPTED FOR PUBLICATION
3 May 2022

PUBLISHED
24 May 2022

PAPER

Electronic properties of twisted multilayer graphene

V Hung Nguyen[1,*], Trinh X Hoang[2] and J-C Charlier[1]

[1] Institute of Condensed Matter and Nanosciences, Université catholique de Louvain (UCLouvain), B-1348 Louvain-la-Neuve, Belgium
[2] Institute of Physics, Vietnam Academy of Science and Technology, Ba Dinh, Hanoi 11108, Vietnam
* Author to whom any correspondence should be addressed.

E-mail: viet-hung.nguyen@uclouvain.be

Keywords: graphene, electronic structure, atomistic modeling

Abstract

Twisted bilayer graphene displays many fascinating properties that can be tuned by varying the relative angle (also called twist angle) between its layers. As a notable feature, both the electronic flat bands and the corresponding strong electron localization have been obtained at a specific 'magic' angle (∼1.1°), leading to the observation of several strongly correlated electronic phenomena. Such a discovery has hence inspired the creation of a novel research field called *twistronics*, i.e. aiming to explore novel physical properties in vertically stacked 2D structures when tuning the twist angle between the related layers. In this paper, a comprehensive and systematic study related to the electronic properties of twisted multilayer graphene (TMG) is presented based on atomistic calculations. The dependence of both the global and the local electronic quantities on the twist angle and on the stacking configuration are analyzed, fully taking into account atomic reconstruction effects. Consequently, the correlation between structural and electronic properties are clarified, thereby highlighting the shared characteristics and differences between various TMG systems as well as providing a comprehensive and essential overview. On the basis of these investigations, possibilities to tune the electronic properties are discussed, allowing for further developments in the field of *twistronics*.

1. Introduction

Twisted multilayer graphene (TMG) refers to structures of vertically stacked graphene layers when one or a few layers are rotated relative to the others by arbitrary angles [1–12], thus creating the so-called moiré superlattices. The first member of TMG systems, twisted bilayer graphene (TBLG), has recently attracted great interest from the scientific community since it exhibits fascinating properties, leading to the exploration of several novel features as surprising as superconductivity that can not be observed in conventional graphene systems [13]. In particular, and most remarkably, electronic properties of TBLG can be tuned by varying the twist angle θ [14, 15], especially leading to the observation of localized flat bands near the Fermi level at a critical angle ($\simeq$1.1°) called 'the magic angle' [16, 17]. At this critical angle, many-body effects are therefore significantly enlarged [18–23] and charge carriers do not possess enough kinetic energy to escape from their strong mutual interactions, thus forming novel strongly correlated electronic states. Such a strong electronic correlation in magic-angle TBLG is the key ingredient for observing several novel phenomena such as superconductivity, correlated insulating states, magnetism, and even quantized anomalous Hall effects [24–33].

The observations mentioned have been considered as real scientific breakthroughs, creating a nascent field of 'twistronics' [34]. Indeed, after the discovery of magic-angle TBLG, the research of other twisted systems has become an emerging topic. In addition to TMG, the explored systems include also twisted superlattices of other 2D layered materials such as graphene on hexagonal boron nitride, graphene on transition-metal dichalcogenide layers, van der Waals moiré superlattices of transition-metal dichalcogenide layers, and so on (e.g. see [35–42] as well as the recent review [43] and references therein). These explorations have also inspired researchers to extendedly apply the twist approach to other physical systems, e.g. magnetic 2D materials [44–48] and photonic layered structures [49–52]. In overall, the properties of those systems are

definitely dependent of their constituting layers and importantly, can be tuned by varying their twist angle, similar to those observed in TBLG. In particular, in the TMG cases, electronic flat bands and accordingly, the strongly correlated electronic phenomena have been similarly observed around their magic angle (e.g. see in [4, 8, 11, 53–55]). Moreover, more tunable possibilities can be observed in TMG [4–6, 8, 9, 26, 56, 57], due to a larger number of layers and the plenty of stacking configurations [58], compared to TBLG. In this context, a comprehensive understanding of the electronic properties of TMG is highly desirable. Some new TMGs [6, 9, 11, 12] have been very recently produced experimentally, and hence their corresponding electronic properties are needed to be more exhaustively clarified. In addition, a good understanding of those twisted systems could be also helpful for research of twisted structures based on other 2D materials.

On the theoretical side, though a large number of works devoted to the electronic properties of some TMG has been reported (e.g. in [15, 34, 53, 54, 59–61]), a systematical study on this subject is however still missing. Remarkably, it has been shown that atomic reconstruction (i.e. the structure relaxation) significantly occurs in TBLG at low angles ($\lesssim 1.1^\circ$), thus strongly influencing their electronic properties, i.e. especially the formation of electronic flat bands as well as the electronic localization pictures [21, 62, 63]. The structural and electronic properties of TBLG also exhibit a strong correlation [63], that explains essentially the corresponding electronic localization features. Fully taking into account the atomic reconstruction effects is therefore mandatory to compute accurately the electronic properties of TMG, which has not been properly considered yet in all works previously published in the literature.

This paper aims to investigate systematically the most common and essential electronic properties of TMG by atomistic calculations, which fully take the atomic reconstruction into account. First, twisted bilayer graphene is investigated to illustrate the overall structural and electronic properties induced by the twisting effects. Some of these properties are commonly observed in other multilayer structures. Afterward, the study focuses on several typical twisted multilayer (more than two graphene layers) systems around their magic angles, at which electronic flat bands and strong electron localization are observed. The correlation between the obtained electronic and structural properties is also clarified. Electronic (both global and local) quantities obtained depending on the twist angle and the stacking configuration are analyzed in details, thus highlighting the shared characteristics and differences between TMGs. Finally, on the basis of these investigations, possibilities to tune these electronic properties are discussed.

2. Modeling methodology

As mentioned previously, the atomic reconstruction is significant and hence taking into account these structural effects is mandatory to model accurately the electronic properties of twisted graphene systems, especially, at small twist angles around and below the magic one. In this work, we used classical force-fields to compute the atomic structure relaxation. More specifically, intralayer forces are computed using the optimized Tersoff and Brenner potentials [64], while interlayer forces are modeled using the Kolmogorov–Crespi potentials [65, 66]. The atomic structure was optimized until all force components are smaller than 0.5 meV/atom and the electronic calculations were then performed. The atomic structure relaxation obtained by this method is shown to be in good agreement with experiments [19, 67–69] as well as the results obtained by other (both quantum and semi-classical) methods [62, 70–72], except that the intralayer equilibrium C–C bond distance is slightly overestimated by $\sim 1\%$ [66].

Similarly to previous works [21, 63], the electronic properties of TMG (schematized in figure 1) were then computed using the p_z tight-binding (TB) Hamiltonians after the structural optimization has been fully achieved. Hopping energies t_{nm} between carbon C-sites are determined by the standard Slater–Koster formula

$$t_{nm} = \cos^2\ \phi_{nm} V_{pp\sigma}(r_{nm}) + \sin^2\ \phi_{nm} V_{pp\pi}(r_{nm}) \tag{1}$$

where the direction cosine of $\vec{r}_{nm} = \vec{r}_m - \vec{r}_n$ along Oz axis is $\cos\phi_{nm} = z_{nm}/r_{nm}$. The distance-dependent Slater–Koster parameters are determined as [73]

$$V_{pp\pi}(r_{nm}) = V^0_{pp\pi}\ \exp\left[q_\pi\left(1 - \frac{r_{nm}}{a_0}\right)\right] F_c(r_{nm})$$
$$V_{pp\sigma}(r_{nm}) = V^0_{pp\sigma}\ \exp\left[q_\sigma\left(1 - \frac{r_{nm}}{d_0}\right)\right] F_c(r_{nm})$$

with a smooth cutoff function $F_c(r_{nm}) = \left[1 + \exp\left(\frac{r_{nm} - r_c}{\lambda_c}\right)\right]^{-1}$.

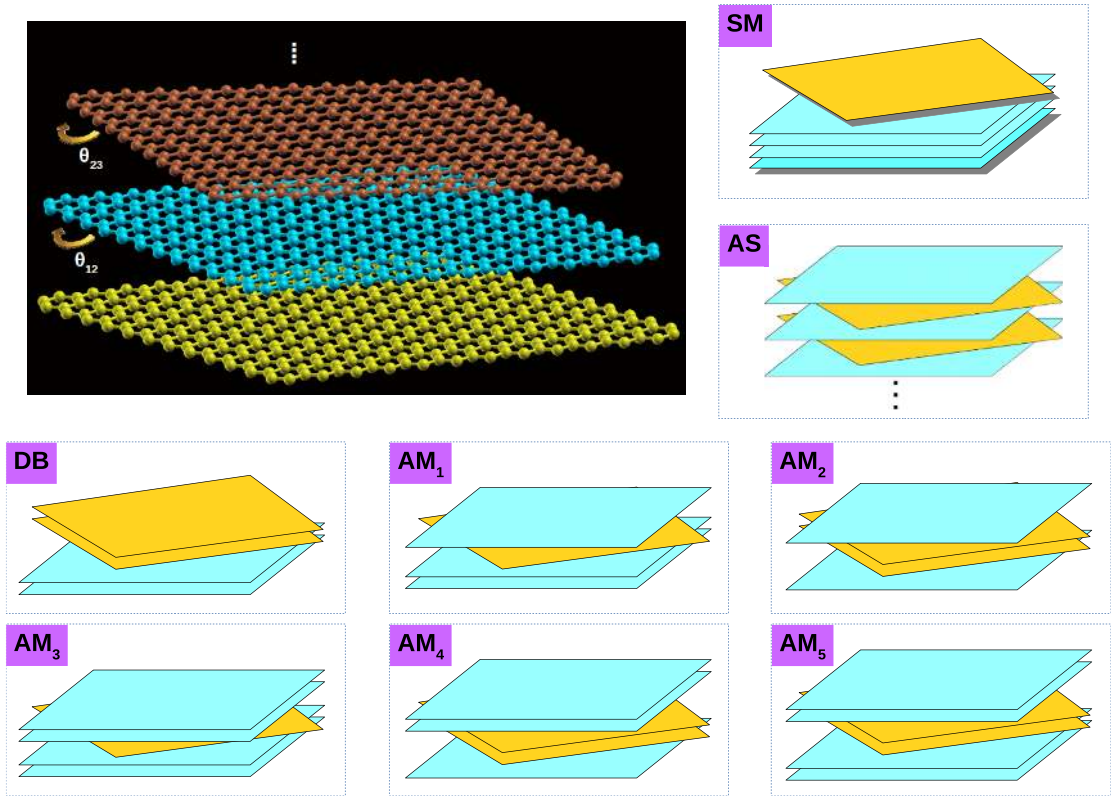

Figure 1. Twisted multilayer graphene systems investigated in this work. SM-structures are twisted systems created by putting and rotating a graphene monolayer on top of a multilayer (n layers) graphene that is either in AB stacked or in ABC stacked. These structures are hereafter abbreviated as SM-$(AB)_n$ and SM-$(ABC)_n$, respectively. AS-structures are alternatively twisted systems of n graphene monolayers, abbreviated as AS_n. DB is the abbreviation of twisted double bilayer graphene superlattices. At last, AM_n structures ($n = 1, 2, 3, 4, 5$) are alternatively twisted systems containing, at least, one Bernal stacking graphene bilayer.

In this work, the TB Hamiltonian was further simplified from the model considered in [63], i.e. only couplings limited by $r_{\text{inplane}} \leqslant 2.16$ Å were taken into account. This approximation presents an advantage that the matrix of TB Hamiltonian is very sparse so as to make calculations feasible for small twist angles and/or multilayer systems in which the number of C atoms could be huge. Within this approximation, the TB parameters [63] are slightly adjusted as follows:

$$\begin{aligned} V^0_{pp\pi} &= -2.7 \text{ eV}, \;\; V^0_{pp\sigma} = 367.5 \text{ meV}, \\ \frac{q_\pi}{a_0} &= \frac{q_\sigma}{d_0} = 22.18 \text{ nm}^{-1}, \\ a_0 &= 0.1439 \text{ nm}, \;\; d_0 = 0.33 \text{ nm}, \;\; r_c = 0.614 \text{ nm}, \;\; \lambda_c = 0.0265 \text{ nm} \end{aligned}$$

Indeed, such an adjusted TB Hamiltonian fairly accurately reproduces the electronic properties of TBLG as obtained in [63] as well as in experiments, e.g. in [21, 23, 24]. As a clear illustration, the almost flat bands near the Fermi level is perfectly reproduced in the relaxed TBLG in the vicinity of the magic angle (i.e. $\sim 1.1^\circ$, see figure 3 below) as experimentally observed (e.g. see in [24]).

3. Twisted bilayer graphene

As the simplest TMG structure, TBLG exhibits most clearly essential electronic properties induced by the twisting effects. These properties as well as their correlation with the structural properties, that generally also appear in other TMGs (as examples, see in [54, 63] as well as illustration in figures 14 and 15 in section 5), will be therefore revised and systematized in this section.

Typical images illustrating the evolution of the stacking structure in TBLG when varying the twist angle θ are presented in figure 2. The stacking vector $\boldsymbol{t}$, as illustrated in the bottom-left panel, indicates the smallest displacement applied locally to one layer to recover the AA stacking at the considered position. In general, TBLG superlattice includes three typical stacking regions: AA stacking, AB/BA stacking regions and soliton lines between AB/BA ones (called SP for 'saddle point'). The presented images illustrate that the magic angle $\sim 1.1^\circ$ separates TBLG into two regimes: $\theta > 1.1^\circ$ (large angles) and $\theta < 1.1^\circ$ (small ones) [63]. At large

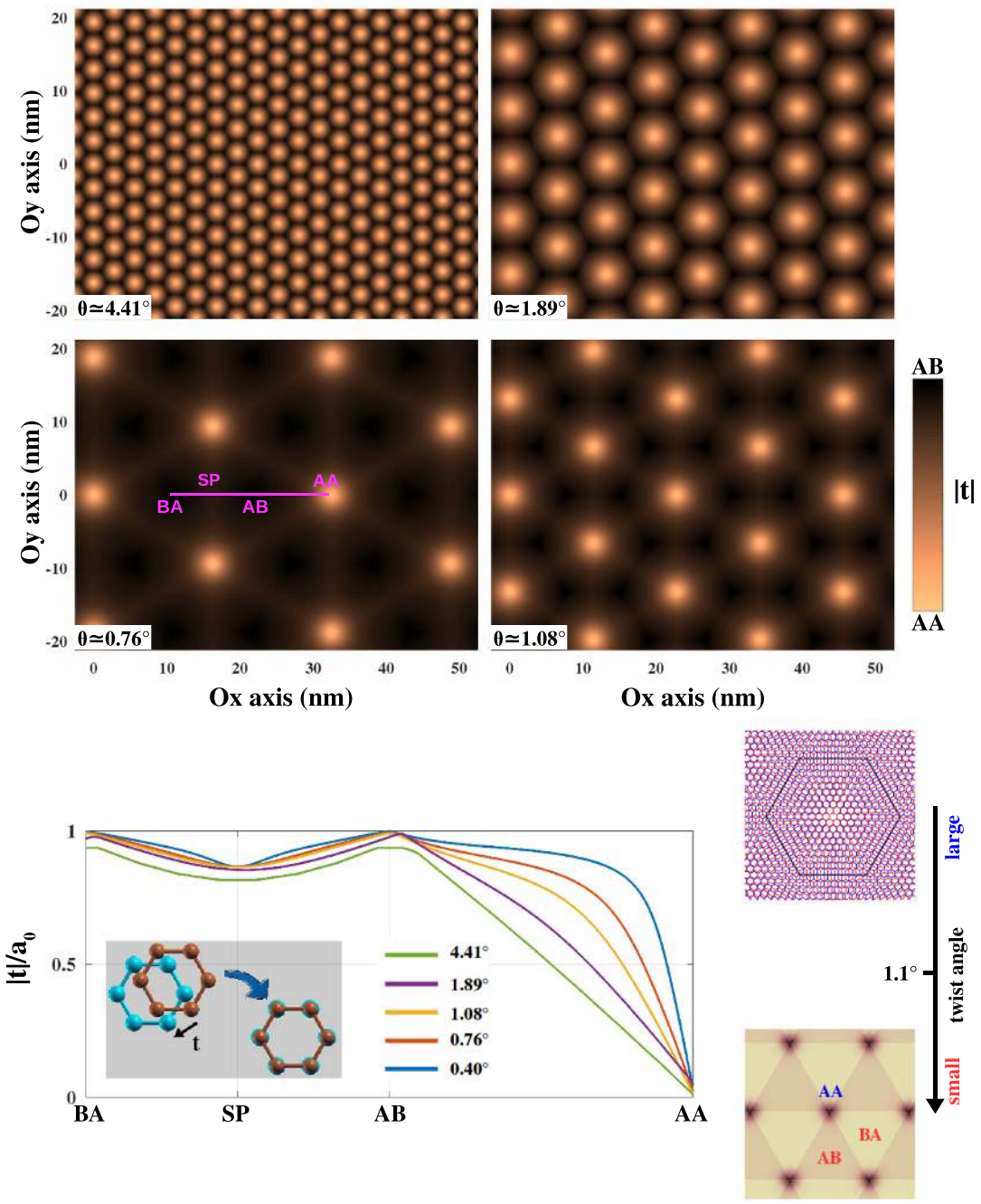

Figure 2. Stacking structure of TBLG imaged by the spatial variation of stacking vector $\boldsymbol{t}$ (as defined in the inset of bottom-left panel) when varying the twist angle θ. Four top images are 2D real-space representation of $|\boldsymbol{t}|$ while the bottom-left one is a plot of $|\boldsymbol{t}|$ extracted along the line connecting BA–SP (soliton line)—AB–AA stacking regions. The bottom-right diagram is a simple description of the stacking properties of TBLG in the different θ-regimes (from large to small twist-angles).

angles, the moiré superlattice evolves smoothly and both AA and AB/BA stacking regions are continuously enlarged when decreasing the twist angle. However, AA stacking regions get saturation when θ decreasingly approaches 1.1°. At small angles, whereas the size of AA stacking regions is unchanged, AB/BA regions are continuously enlarged when decreasing θ, according to the enlargement of moiré cells. Thus, in addition to the critical angle (i.e. magic angle) ∼1.1°, there are two TBLG classes, separated by such angle and exhibiting distinct stacking structures, as summarized in the bottom-right diagram of figure 2.

The structural properties discussed above crucially govern the electronic features of TBLG, as illustrated by the typical electronic structures in figure 3 as well as the local densities of states (LDOS) images in figure 4. In large-angle TBLG, Dirac fermions are still preserved at low energies but a remarkable renormalization of their Fermi velocity is obtained [74], as seen in figure 3 for $\theta \simeq 2.28°$. In addition, saddle points emerge at the crossing of Dirac cones (i.e. at the M-point in the superlattice Brillouin region), yielding van Hove singularities in the density of states (DOS) at energies that are lowered down when decreasing θ.

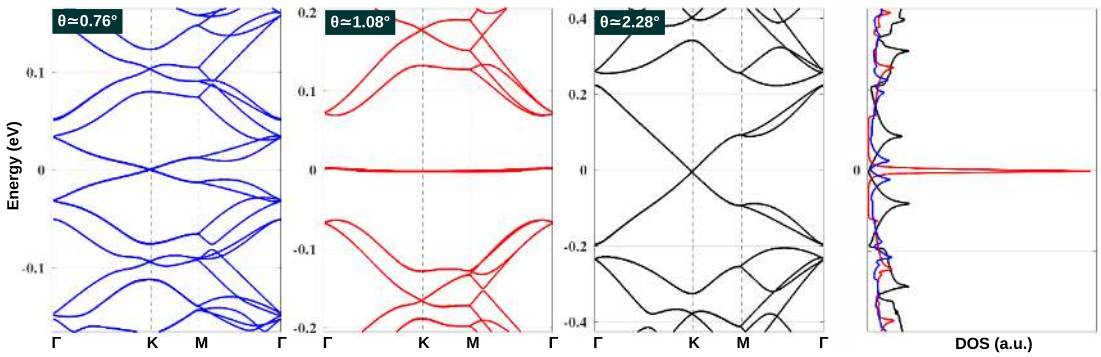

Figure 3. Electronic bandstructure of TBLG for the twist angle $\theta < 1.1°$ (left in blue), $\theta \simeq 1.1°$ (center in red) and $\theta > 1.1°$ (right in black). The corresponding density of states (DOS) are presented on the extreme right with the same color scale for the three moiré structures.

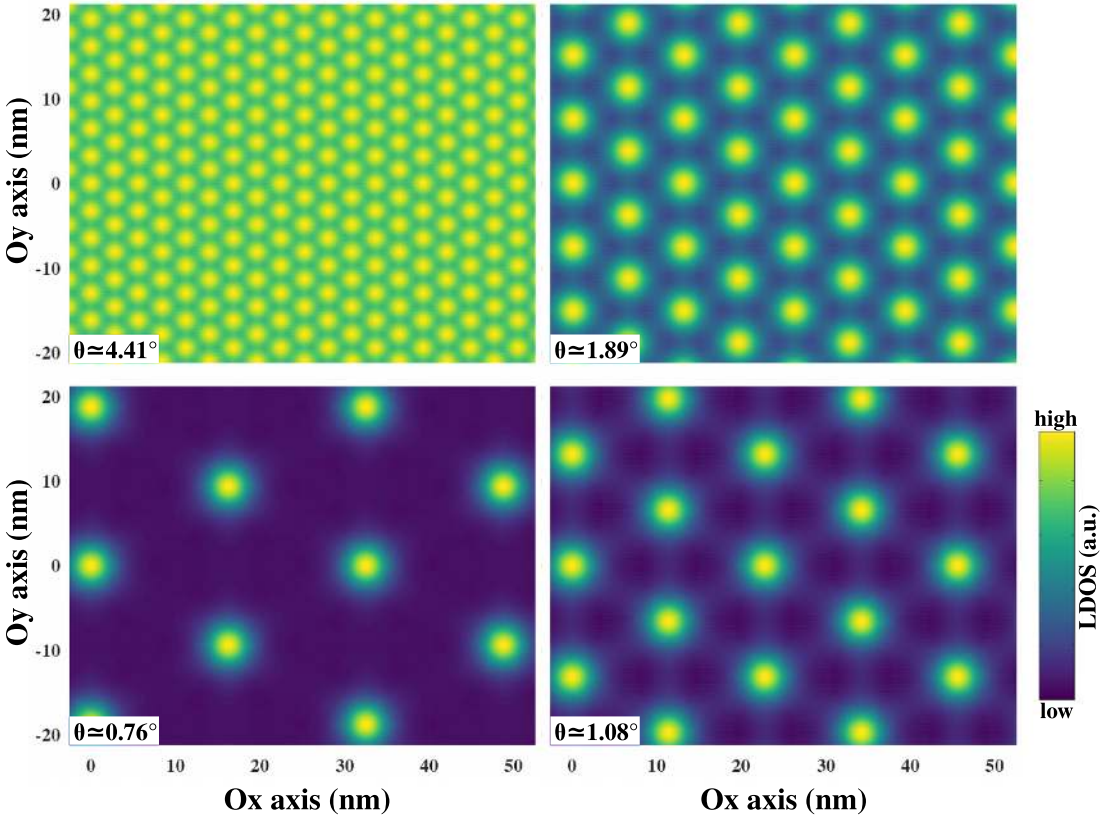

Figure 4. Real-space LDOS images in TBLG at different twist angles. Energy is fixed where the strongest electronic localization is obtained, i.e. at the van Hove singularity point in DOS (see figure 3) for $\theta > 1.1°$ and at zero energy for $\theta \lesssim 1.1°$.

When θ approaches 1.1°, two (electron and hole) van Hove singularities merge at zero energy and accordingly the low energy bands are flattened, resulting in the observation of an extremely high DOS peak at that energy (see figure 3 for $\theta \simeq 1.08°$). The angle 1.1° has been thus called the 'magic angle' [16]. When further decreasing θ, the electronic bands become more dispersive again (see figure 3 for $\theta \simeq 0.76°$). Remarkably, it has been shown that fully taking the structure relaxation into account, the electronic flat band (accordingly, the localized DOS peak at zero energy) as at 1.1° is no longer observed for small angles <1.1° as discussed in details in [63]. Moreover, even though it is not present in the global electronic quantities, the strong electronic localization is still observed locally in AA stacking regions, which has been experimentally confirmed in [21].

These distinct electronic properties of TBLG at large and small angles are visually illustrated by the LDOS pictures in figure 4 as well as their correlation with the structural properties discussed in figure 2. Actually, the LDOS in figure 4 are represented in each case at the strongest localization point. First, the strong

electronic localization is observed in the AA stacking region for all twist angles. Remarkably, the real-space electronic localization exhibits the similar θ-dependence, compared to that of stacking structure presented in figure 2. Indeed, while it is continuously enlarged when reducing θ above 1.1°, the real-space LDOS peak obtained in AA stacking regions is maximum at $\theta \simeq 1.1°$ and saturates in the regime $<1.1°$. These results demonstrate clearly a strong correlation between the structural properties and the electronic localization features in TBLG.

More remarkably, the observation of electronic flat bands is found to be essentially related to the maximum electronic localization in AA stacking regions and their maximum contribution to the global electronic properties of the system (see also discussions in section 5). These features are concurrently obtained at $\theta \simeq 1.1°$. To clarify such observation, we notice additionally here that the strongest electronic localization in energy is favorable (unfavorable) in AA stacking regions (other stacking regions) [63]. At large angles $>1.1°$, the electronic localization in AA stacking regions (see figure 4 for $\theta \simeq 4.41°$) and consequently the global localization in energy (see the extreme right panel of figure 3) are relatively weak. When decreasing θ in this regime, the electronic localization in AA stacking regions and their contribution are continuously enhanced. Accordingly, global localization (i.e. DOS) peaks increase and their positions concurrently move towards zero energy. At $\theta \simeq 1.1°$, all these effects are maximized and consequently the electronic flat bands are obtained. When further decreasing θ in the regime below 1.1°, even though a strong electronic localization is still locally observed in the saturated AA stacking region, the increasing contribution of AB/BA stacking ones gradually diminishes the global electronic localization and hence flat bands can not be observed again [63], thus precluding the emergence of other (i.e. small) magic angles predicted by other theoretical calculations [16].

Finally, it is worth noting that even though they could be quantitatively affected by the presence of a larger number of layers and/or by a more complicatedly stacked configuration, the structural and electronic features similar to those presented above are still observed in other TMGs, simply because all these features are essentially governed by twisting effects.

4. Twisted multilayer graphene

The electronic properties of twisted graphene systems containing more than two layers as schematized in figure 1 are now investigated. The creation of these systems could be simply considered as adding one or a few graphene layers to a TBLG one. Since these TMG share a similar θ-dependence with TBLG (e.g. as seen in [54, 63]), the present study is mainly focused on the magic-angle cases where low-energy bands are most flat and thus strongly correlated electronic phenomena can be observed.

4.1. Rotated graphene monolayer on graphene multilayer

We first consider TMG obtained when one rotated graphene monolayer is placed on top of a graphene multilayer (i.e. SM-systems in figure 1) as recently achieved experimentally in [12]. Their electronic bandstructures are presented in figure 5 in both cases when the graphene multilayer is either in an AB-stacked form or in an ABC-stacked one.

First of all, the SM-$(AB)_2$ (i.e. twisted monolayer-bilayer) system at its magic angle exhibits a bandstructure (see on top of figure 5) with isolated flat bands, similar to that obtained in the magic-angle TBLG. The main difference between two cases is that these bands (accordingly, zero-energy DOS peak) are observed to be less flat (lower) than those of TBLG. Note that continuum Hamiltonian calculations [55] have shown that the bandwidth of flat bands in SM-$(AB)_2$ system is generally narrower than that obtained in magic-angle TBLG. This is indeed also confirmed by our calculations for systems at the same twist angle in the regime $\theta \gg 1.1°$. The results in the magic angle case however exhibit an opposite behavior, i.e. the bandwidth of the magic-angle SM-$(AB)_2$ system is larger than that obtained in magic-angle TBLG. This is actually consistent with the results presented in [20, 56] for atomic reconstructed superlattices. These results could be understood as a consequence of the fact, as discussed in the previous section, that the band flatness has a strong correlation with the real-space electronic localization that is basically stronger in AA-stacking regions [63]. In SM-$(AB)_2$ systems, the corresponding regions are obtained in an AAB-stacked form, i.e. a mixture of AA- and AB-stacking configurations while the latter is unfavorable for the electronic localization. Such mixture diminishes the electronic localization in the SM-$(AB)_2$ system. This is visibly illustrated by comparing the total LDOS in figure 6 with that obtained in magic-angle TBLG (see figure 4 for $\theta \simeq 1.08°$) and is further demonstrated in figure 14 in section 5, thus explaining essentially the less flat bands obtained in the SM-$(AB)_2$ case.

In addition, another interesting feature is found in figure 6 that flat bands in the magic-angle SM-$(AB)_2$ system exhibit a coexistence of layer-resolved localized-delocalized behaviors, i.e. they are spatially localized on the twisted side whereas delocalized on the bilayer side. This unique feature has been also experimentally

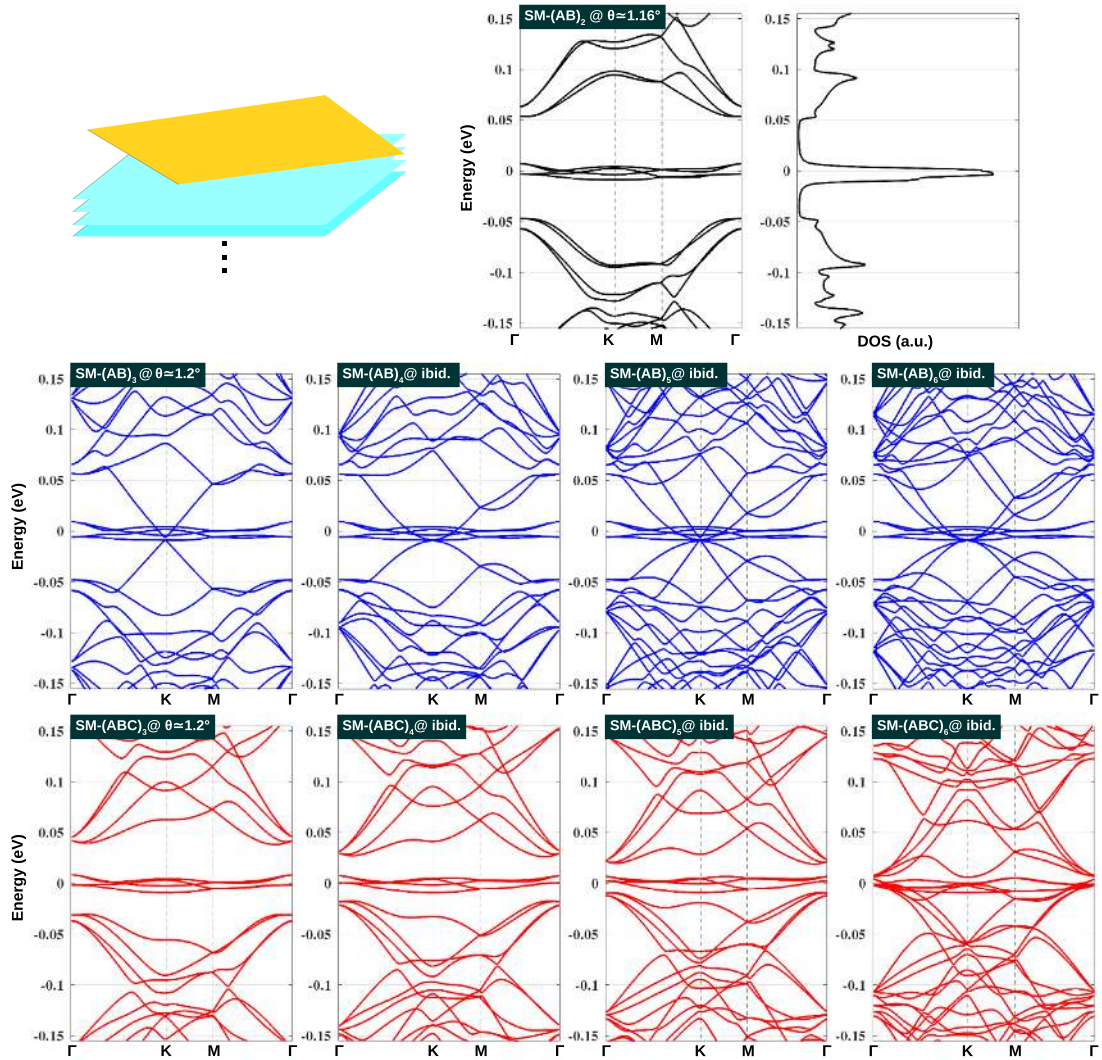

Figure 5. Electronic bandstructures of different SM-systems at their magic angle. On top, the results in SM-$(AB)_2$ (i.e. twisted monolayer-bilayer) structure are presented. Other systems including SM-$(AB)_n$ and SM-$(ABC)_n$ (see the definition in figure 1) at their magic angle $\sim 1.2^\circ$ are computed and presented in the second and third rows, respectively, with $n = 3, 4, 5, 6$ (from left to right). On top-right, DOS versus energy in SM-$(AB)_2$ structure is also superimposed.

confirmed in a recent work [75] and the delocalized correlated electronic states have been similarly explored in twisted double bilayer graphene [76]. Note that electronic states delocalized either in the graphene plane or in different layers are generally obtained in twisted systems consisting of more than two layers as the SM-$(AB)_2$ system here and others considered below, where certain layers are strongly influenced by the moiré superlattice interactions whereas the weak effects take place in other layers. Moreover, the observed coexistence of localized-delocalized electronic states essentially has a tight relationship with the weak real-space localization in the SM-$(AB)_2$ system discussed above.

When the number of graphene layers of the multilayer counterpart increases, both systems SM-$(AB)_n$ and SM-$(ABC)_n$ exhibit clearly distinct electronic properties (see figure 5). In particular, while the electronic structure of SM-$(AB)_n$ systems presents both flat bands and dispersive ones at low energies, flat bands in SM-$(AB)_n$ systems are still clearly isolated from high-energy bands for $n \leqslant 5$. However, the energy gaps between the mentioned bands in the latter case is reduced when increasing n and is closed for $n > 5$. Such distinct properties could be explained by the difference in electronic properties of AB- and ABC-stacked graphene multilayer systems, i.e. while ABC-stacked systems host a single band that is partially flat around zero energy, there is a mixture of several (increasing with n) parabolic and linear bands in the AB-stacked ones [77].

To further clarify the difference between these two systems, we analyze their layer decomposed DOS (LD-DOS) in function of energy in figure 7. For the SM-$(AB)_2$ system, besides the coexistence of layer-resolved localized-delocalized states presented in figure 6, LD-DOS still exhibits the usual behaviours similar to that observed in magic-angle TBLG. However, other distinct features are found for SM-systems

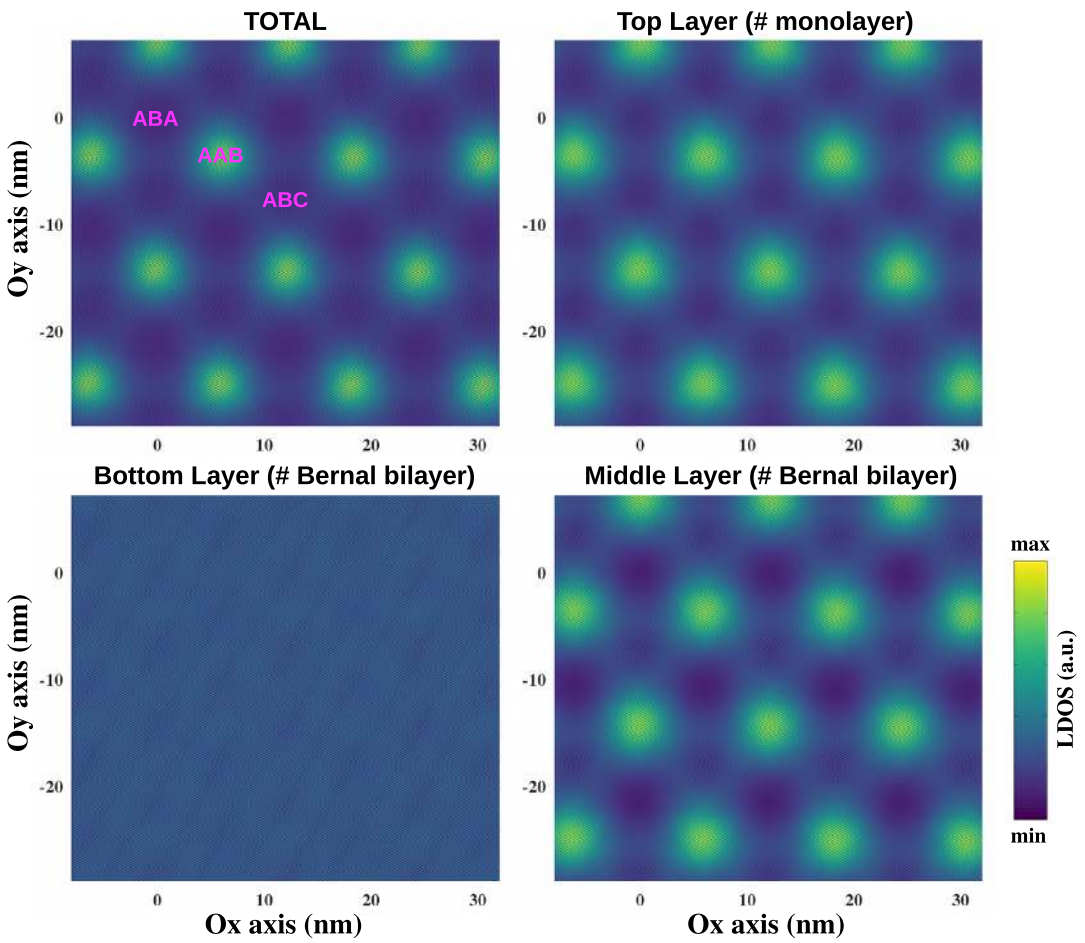

Figure 6. Total LDOS and layer decomposed LDOS in SM-$(AB)_2$ system in figure 5 at zero energy.

with a larger number of graphene layers. In particular, the electron localization is mostly observed in three top layers of SM-$(AB)_n$ structures where the moiré superlattice interactions take place. However, the localization is obtained in both top and bottom outermost layers of SM-$(ABC)_3$ and SM-$(ABC)_4$ systems (see illustration in figure 7 for SM-$(ABC)_4$ one). Moreover, when the number of layers n further increases, such electron localization in SM-$(ABC)_n$ surprisingly changes, i.e. the effect in the top outermost layers is diminished while it is enhanced in the bottom ones. When n is large enough, the electron localization is mostly observed in the bottom outermost layers as illustrated in figure 7. for the SM-$(ABC)_6$ system.

4.2. Alternatively twisted graphene monolayers

TMGs created by alternatively rotating $(0, \theta, 0, \theta, \ldots)$ graphene monolayers (i.e. AS_n structures in figure 1) have been also very recently obtained experimentally and shown to exhibit several novel strongly correlated phenomena [6, 7, 9, 11, 53, 78] . The magic angle of these AS_n structures can be estimated by the simple expression $\theta_n^{MA} = 2\,\theta_n^{MA}\cos(\pi/(n+1)))$ with $\theta_2^{MA} \simeq 1.1^\circ$ as proposed in [11, 53]. This is indeed demonstrated in figure 8 where (almost) flat bands are obtained in AS_n structures near θ_n^{MA}. However, different from the results suggested by the effective continuum models [6, 9, 11, 53], the TB bandstructure here presents four degenerate flat bands (more visibly seen in section 5 when a vertical electric field is applied) and n–2 additional linear bands at low energies. Moreover, saddle points (accordingly, van Hove singularities in DOS) occur in dispersive bands for $n \geqslant 4$. The low-energy bands in these AS_n systems are also shown to be generally flatter than those obtained for the SM-structures presented in figure 5, thus confirming again our discussion above about the property of electron localization in the presence of Bernal stacking bilayer graphene. Note that another difference between systems without and with Bernal stacking bilayer graphene has been also discussed in [20]. Indeed, in this study, significant sublattice polarization has been observed in the latter case, leading to weaker electron-phonon couplings than those obtained in twisted systems of graphene monolayers only.

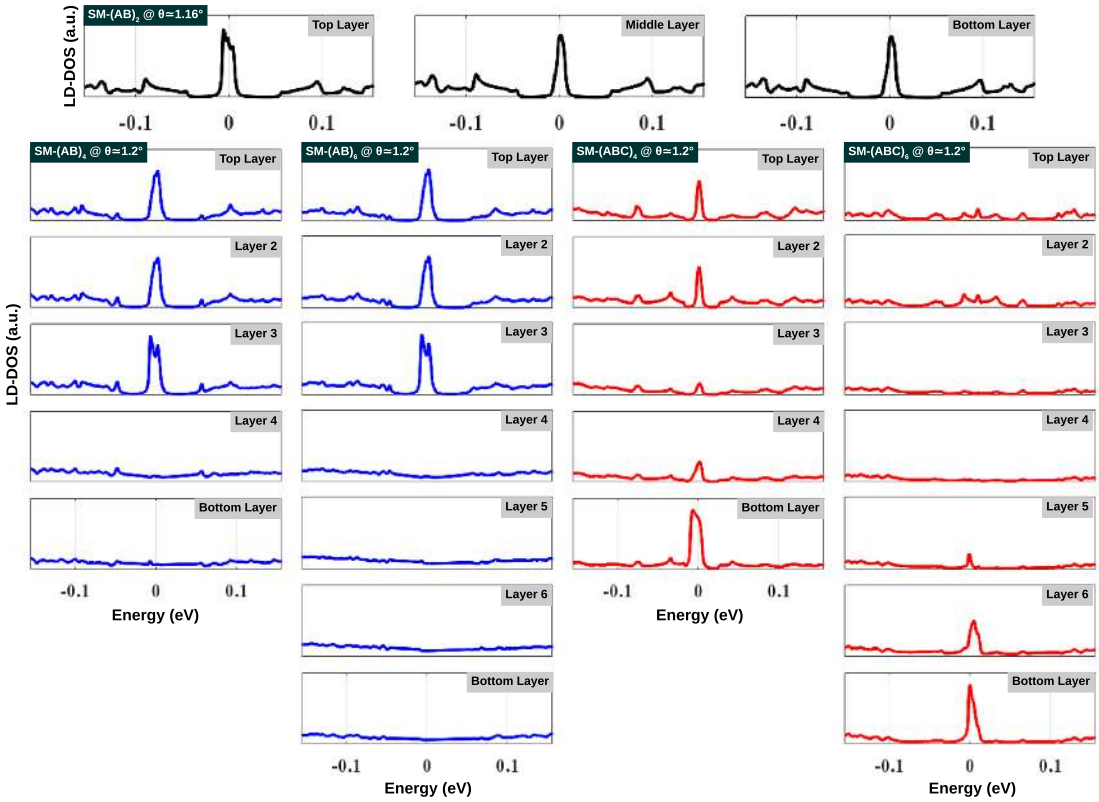

Figure 7. Layer decomposed DOS (LD-DOS) in some SM-systems considered in figure 5.

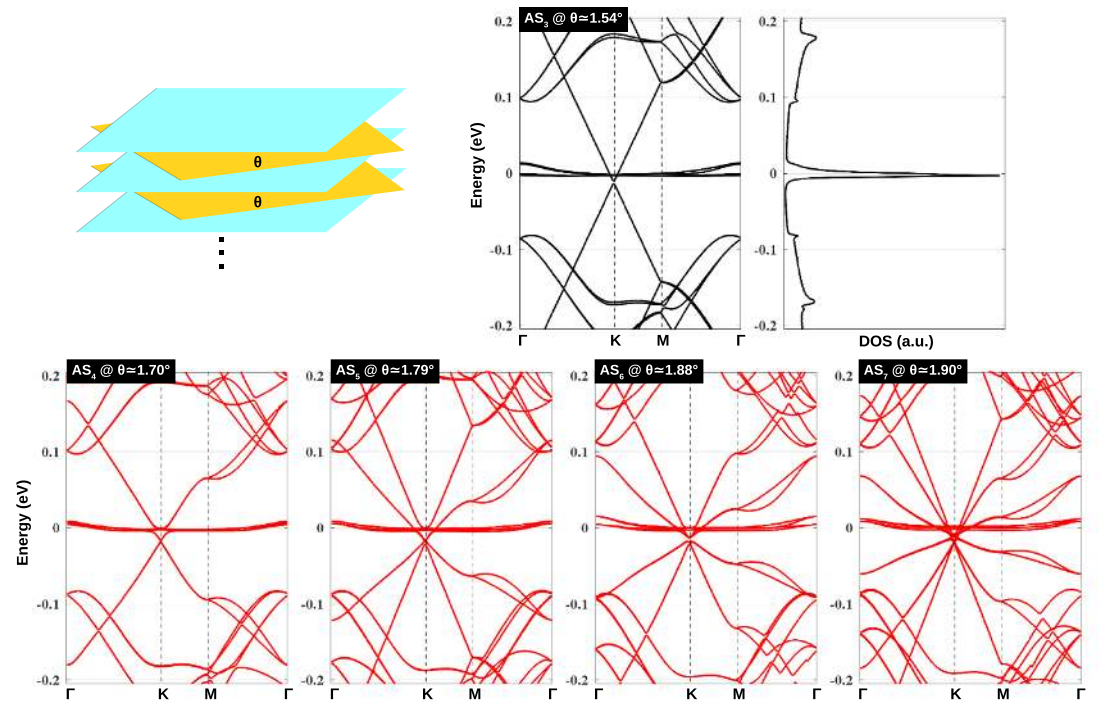

Figure 8. Electronic bandstructures of alternatively twisted systems of graphene monolayers schematized on top-left (i.e. the AS_n systems specified in figure 1) with θ near their magic angle θ_n^{MA} (see text). On top-right, DOS versus energy in AS_2-structure is also superimposed.

To understand more deeply their electronic properties, the layer decomposed DOS obtained in these AS_n structures is presented in figure 9. Remarkably, the strong electronic localization takes place in their centered layers, in contrast to those observed in SM-ones presented in figure 7. Moreover, LD-DOS in the centered

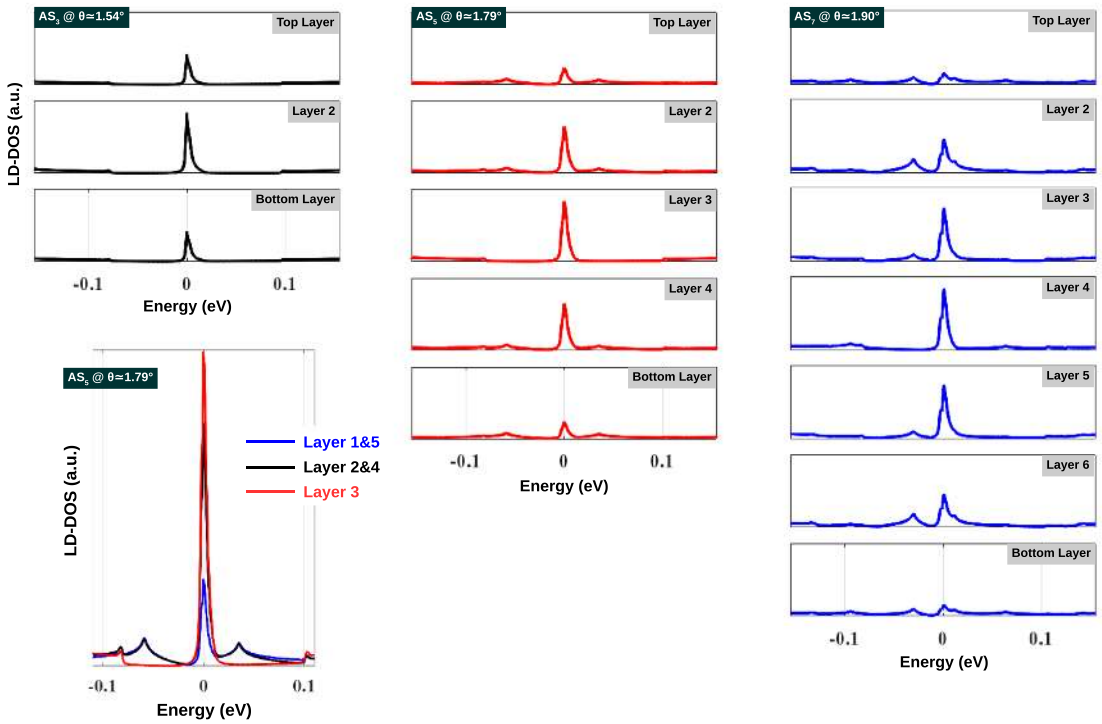

Figure 9. Layer decomposed DOS (LD-DOS) in some AS-systems considered in figure 8. On bottom-left, a zoom-combined picture of the results in AS_5 structure is presented.

layers presents behaviors that are very similar to those obtained in magic-angle TBLG. In particular, the strongly localized DOS peak is likely isolated from high-energy electronic states by finite energy gaps. Contrastingly, LD-DOS in other layers (especially, the outermost ones) exhibit some signatures of dispersive bands, i.e. the characteristics of linear bands and van Hove singularities induced by the twist as visibly shown in the zoom-image on the bottom of figure 9. Thus, the flat bands and dispersive ones of AS_n structures exhibit oppositely spatial properties, i.e. whereas the former is localized in the system center, the latter is observed in outer layers. This implies that there is aslo a coexistence of localized-delocalized electronic states in the AS_n systems of large n.

When AS_n systems are created, another remarkable possibility could in principle be obtained, in particular, one or a few graphene layers are rotated by $\theta_{60} = \theta + 60^\circ$ (instead of θ) as illustrated on top of figure 10, similar to that reported in [79] for graphene/hBN structures. Actually, such θ_{60}-rotations do not change the lattice orientation of the graphene layer, compared to the simple θ-rotated systems considered in figures 8 and 9. However, three AAA-, ABA- and BAB-stacking regions obtained in the latter case are changed to AAB-, ABB- and ABC-stacking ones in the AS_n systems with $\theta + 60^\circ$ rotations, leading to significant changes in their electronic structure. Indeed, the flat electronic bands are observed at another twist angle as shown in figure 10, compared to similar structures (i.e. with the same number of layers) presented in figures 8 and 9. In addition, dispersive bands at low energies are generally no longer linear ones. These changes can be clarified by analyzing the structural properties of two considered types of AS_n systems (e.g. see in figure 11 for the AS_3 cases). In particular, when compared to the first type (i.e. with θ rotations only), the top layer of the AS_3 system in figure 10(a) presents a totally different buckling pattern (see the top panels in figure 11). Similarly, the middle layer of the latter system is no longer flat as that observed in the former one (see the panels in the second row of figure 11). Accordingly to these different structural properties, these two systems exhibit totally different LDOS images as shown in the bottom of figure 11. These results thus clarify the difference in their electronic structures discussed above.

4.3. Other TMG systems

In the presence of Bernal stacking graphene bilayer, more complicated TMGs can be created as illustrated in figure 1, including twisted double bilayer graphene (DB-system) and alternatively twisted structures (AM_n-ones with $n = 1, 2, 3, 4, 5$). Their electronic bandstructures at the magic angle are presented in figure 12. First, the isolated flat bands are only obtained in magic-angle DB-structure [54], similar to those

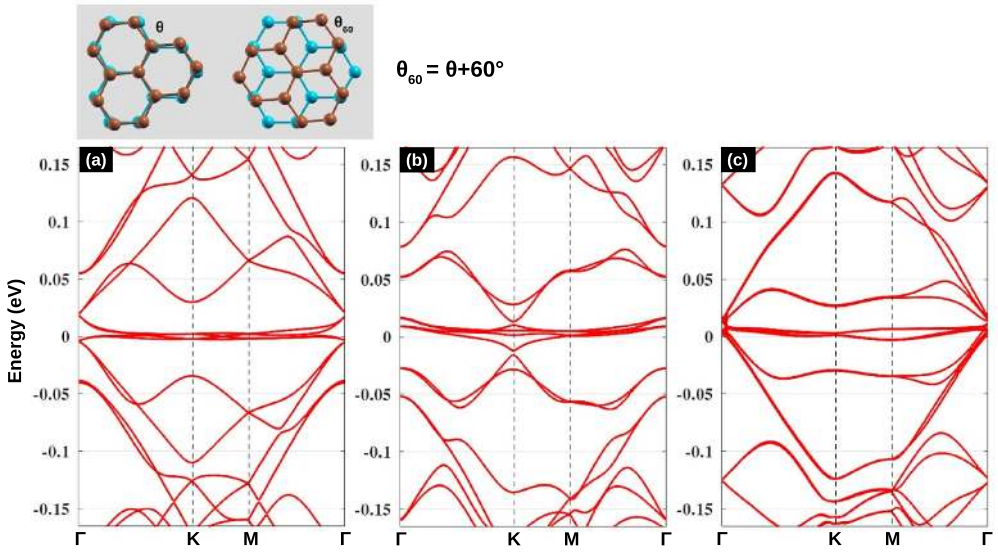

Figure 10. Electronic bandstructures of AS_n systems when one or a few layers are additionally rotated by 60° (see the illustration on top). In (a) and (b), the top layer of AS_3 at $\theta \simeq 1.30°$ and AS_4 at $\theta \simeq 1.54°$, respectively, is additionally rotated by 60°. In (c), such additional 60°-rotation is applied to two top layers of AS_4 at $\theta \simeq 1.35°$.

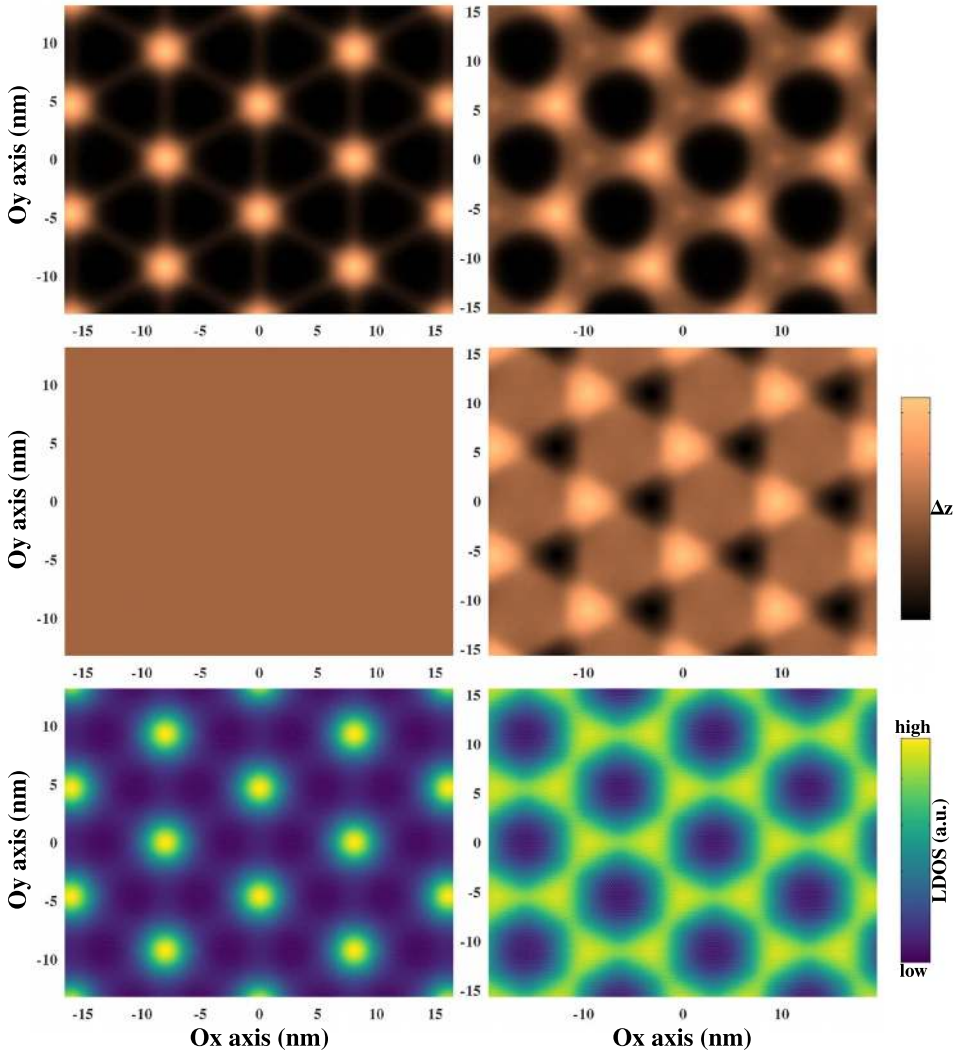

Figure 11. The structural and electronic properties of two AS_3 structures: AS_3 at $\theta \simeq 1.54°$ in figure 8 (see in the left) and AS_3 at $\theta \simeq 1.30°$ considered in figure 10(a) (see in the right). Images in the first and second rows present the spatial variation of out-of-plane displacements in the top and middle layers, respectively. LDOS of two systems at zero energy is presented in the bottom images.

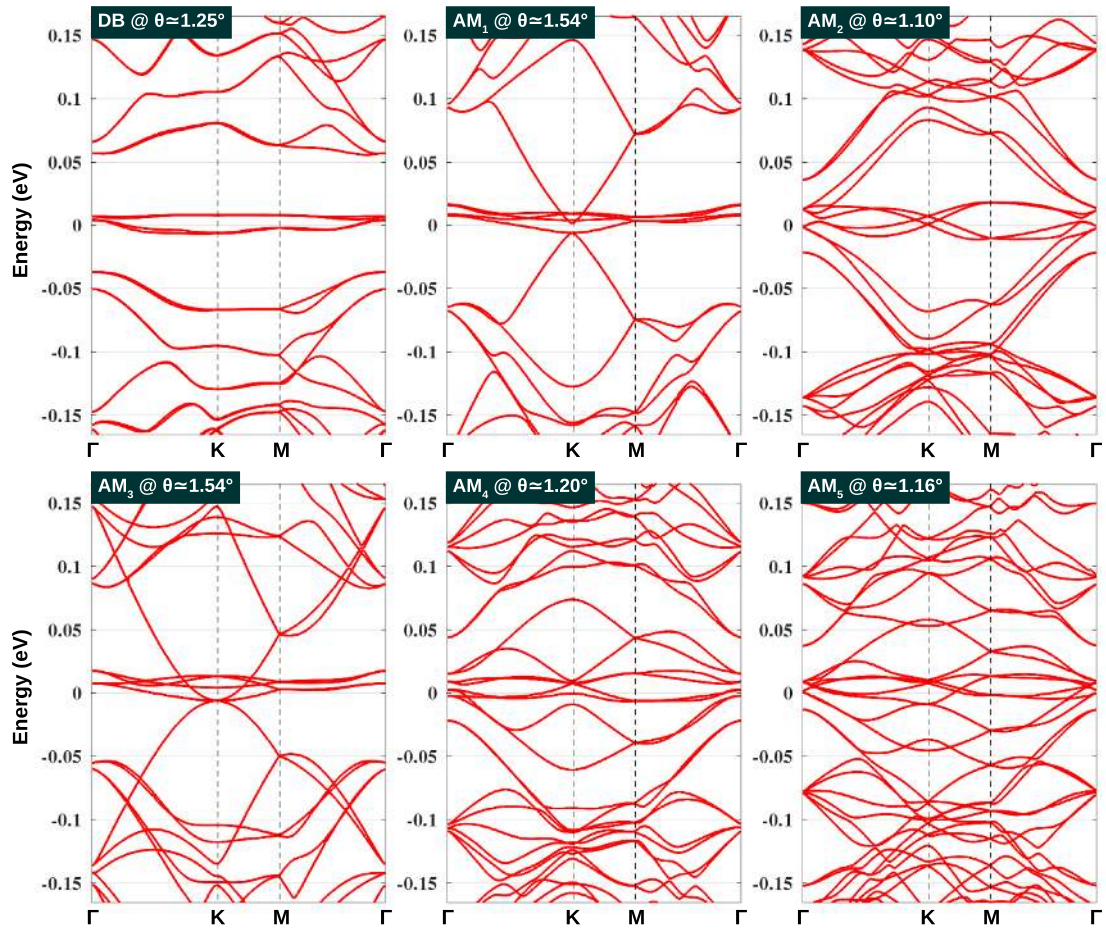

Figure 12. Electronic bandstructures of TMGs including DB- (i.e. twisted double bilayer graphene) and AM-structures (alternatively twisted structures containing, at least, one Bernal stacking bilayer, as schematized in figure 1). Calculations were performed at their magic angles where low-energy bands are most flat.

obtained in TBLG and in SM-$(ABC)_n$ ones with $n \leqslant 4$. In the case of AM_n-systems, the flat bands can be more easily obtained if the middle layer is a graphene monolayer (i.e. AM_1 and AM_3 ones), whereas the low-energy bands are generally less flat if it is a Bernal stacking bilayer. In addition, similar to the AS_n-structures, dispersive bands are always additionally obtained at low energies, which is likely an inherent property of alternatively twisted systems. Once more, the low-energy bands of those systems in the presence of Bernal stacking bilayers are shown to be less flat than those presented above for systems of graphene monolayers only.

For completeness, we investigate in figure 13 the electronic bandstructures of moiré-of-moiré graphene superlattices, that can generally be obtained when different twist angles between adjacent layers are applied. An example presented here is trilayer graphene created by vertically stacking magic-angle TBLG (i.e. $\theta_{12} \simeq 1.08°$) and one rotated (by the angle θ_{23}) graphene monolayer. We particularly consider two cases: a large angle $\theta_{23} \simeq 23.96°$ and a small one $\theta_{23} \simeq 3.25°$. Actually, when θ_{23} is large, the interaction between the graphene monolayer and the magic angle TBLG has no significant effect at low energies, i.e. the obtained low-energy bands are approximately a simple combination of the bands of those two systems. This feature is very similar to those obtained in TBLGs in the large angle regime when their low-energy bands can be considered as a combination of the linear bands of two graphene monolayers. However, when θ_{23} is small (i.e. 3.25° considered here), the mentioned interaction has significant effects on the electronic structure, in particular, the bandwidth of flat bands is significantly enlarged, compared to that obtained in magic-angle TBLG. These results suggest that besides twisted graphene systems investigated above, other more complicated twisted multilayer ones, forming moiré-of-moiré superlattices, shall generally exhibit more complicated electronic structures with less opportunity for observing the flat bands and accordingly, strong electron localization.

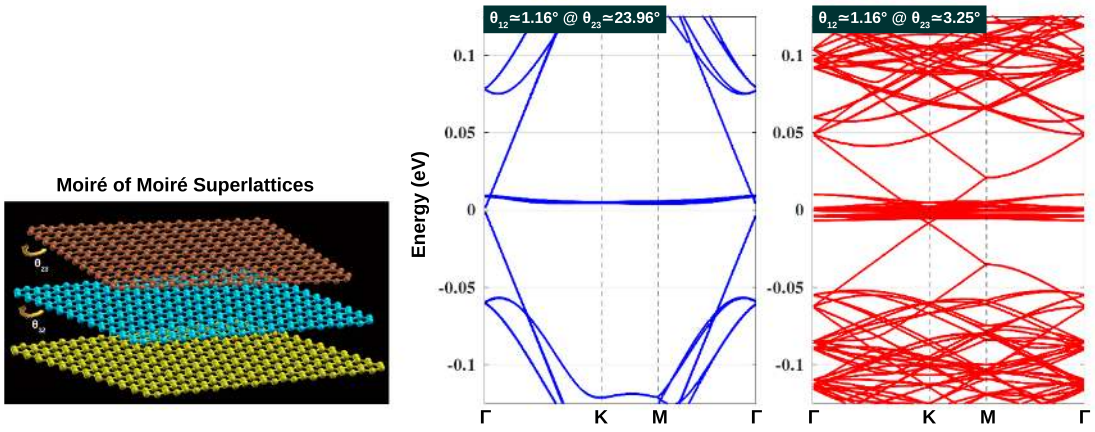

Figure 13. Electronic bandstructures of moiré of moiré graphene superlattices created by putting one rotated (by θ_{23}) graphene monolayer on top of magic-angle TBLG (i.e. $\theta_{12} \simeq 1.08°$). Two typical cases, particularly, large angle ($\theta_{23} \simeq 23.96°$) and small angle ($\theta_{23} \simeq 3.25°$), are presented.

5. Flattening electronic bands and tunability

As emphasized in section 3, the electronic flat bands in reconstructed TBLG is essentially obtained in the situation when the real-space localization in AA stacking regions and their contribution to the global electronic properties are concurrently maximized at the magic angle. In fact, as it will be demonstrated below, such feature is commonly observed in TMGs and hence could be considered as the practical origin of their observed flat bands.

First, it is worth reminding that based on continuum models [16], the first magic angle of TBLG can be estimated using the equation

$$\theta_{\mathrm{MA}} \approx 3w/(2\pi t) \tag{2}$$

where w and t stand for interlayer and intralayer tunneling strengths, respectively. Indeed, $\theta_{\mathrm{MA}} \approx 1.1°$ is obtained, in very good agreement with experiments [21, 23, 24, 26], with $w = 0.109$ eV and $t = 2.7$ eV. Calculations using continuum models [16, 53] have additionally predicted a discrete series of other magic angles $<1.1°$. However, in agreement with the existing experiments (most clearly, see recent articles [21, 23]), atomistic calculations have demonstrated in [63] and as discussed in section 3 that these small magic angles can not be practically obtained in reconstructed TBLGs. This is essentially due to the fact that while it gets maximum at $\theta \simeq 1.1°$, the global electronic localization is progressively reduced, according to the increasing contribution of AB/BA stacking regions when reducing θ below $<1.1°$ as seen in figure 4 and more visibly in the left-panel of figure 14. Interestingly, all these features are similarly observed in other TMGs as seen in two examples, i.e. AS_3 and SM-$(AB)_2$ systems, presented in figure 14. Indeed, their electronic flat bands (i.e. magic angle) are exactly obtained when the real-space localization in AAA and AAB stacking regions, respectively, and their contribution to the global electronic properties of the system are concurrently maximized. Moreover, the commonness of such observation is further emphasized as it is also valid in TMGs when in-plane strains and/or vertical pressure are applied to tune the magic angle value (see figure 15, especially, the full illustration in figures 15(a)–(d)). On the basis of those results, we thus conclude that the maximization of real-space electronic localization in regions where the AA stacking configuration is presented could be considered as the essential origin of the flat electronic bands observed in TMGs.

In addition, the results in figure 14 are another illustration of feature discussed above that at their magic angles, the real-space electronic localization in the presence of Bernal bilayer graphene (i.e. the SM-$(AB)_2$ structure here) is significantly weaker than that in the systems of graphene monolayers only. This feature explained why less flat bands (accordingly, smaller localized DOS peak in energy) are obtained in magic-angle systems containing Bernal bilayer graphene, compared to other structures.

As mentioned, the dependence of magic-angle θ_{MA} on interlayer and intralayer tunneling strengths described in equation (2) suggests that θ_{MA} can be tuned by modifying w and t, for instance, by applying in-plane strains and vertical pressure [26, 78, 80–84] as illustrated in figure 15. In particular, the intralayer hopping energies are reduced by a tensile in-plane strain while the interlayer tunneling strength increases

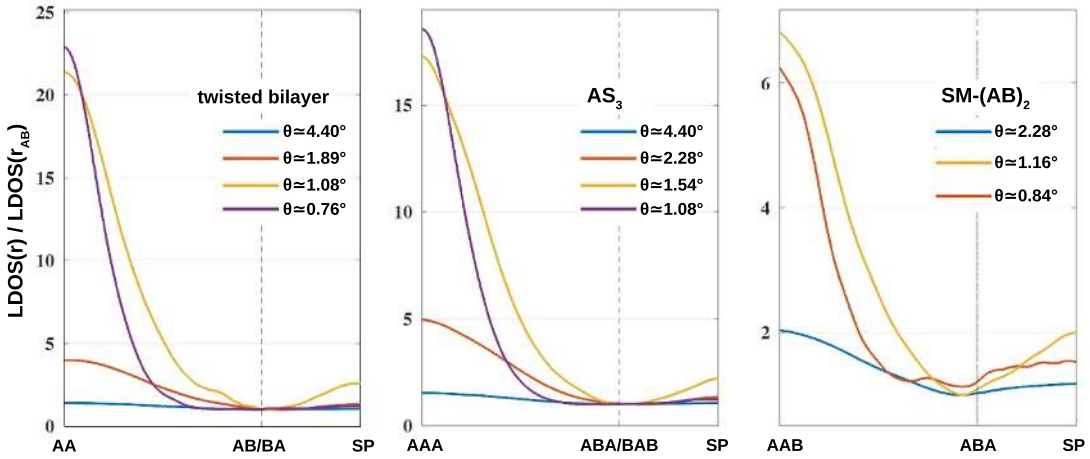

Figure 14. Spatial variation of LDOS in TBLG, AS_3 and SM-$(AB)_2$ systems when varying the twist angle around their magic one. The presented LDOS is extracted along the line connecting regions where AA, SP, AB/BA stacking configurations occur. Calculations are performed at energy where the strongest electronic localization is obtained, i.e. at the electron van Hove singularity point for large θ and at zero energy for θ below the magic angle.

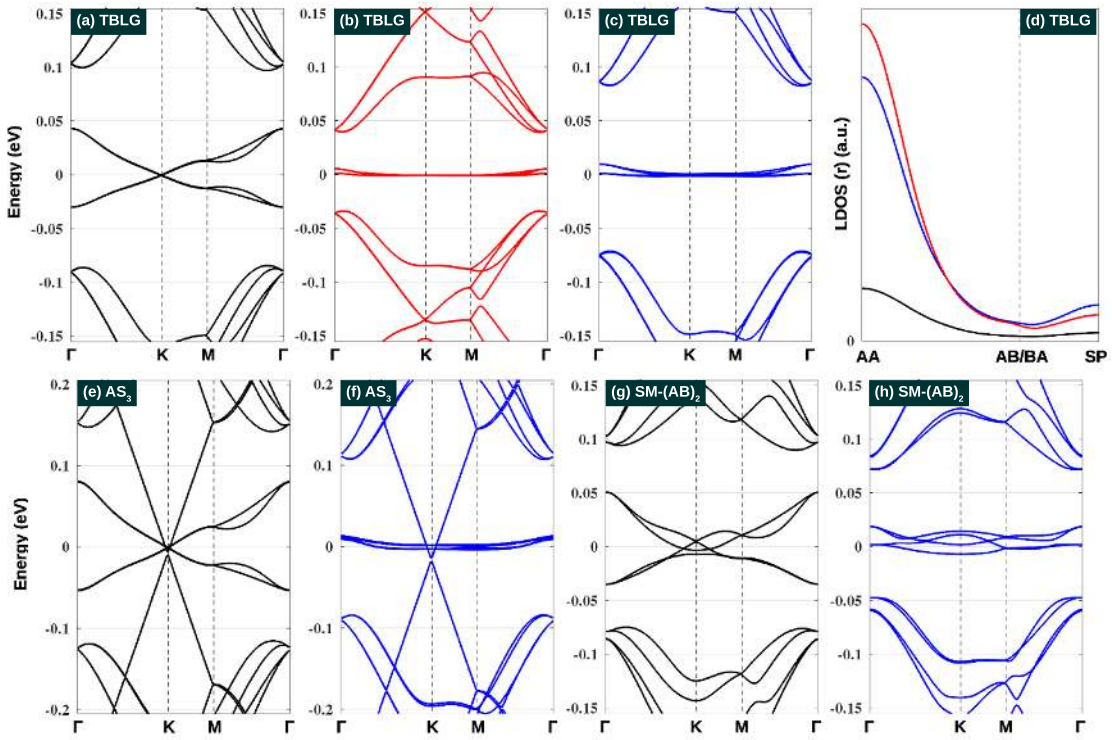

Figure 15. Electronic structures of TMGs modulated by strain and vertical pressure. TBLG at $\theta \simeq 1.30^\circ$ is considered in (a) for the pristine case, in (b) with a biaxial strain of 9%, and in (c) with a vertical pressure $P \simeq 1.45$ GPa. The corresponding LDOS obtained at the strongest electronic localization point is presented in (d). Electronic bandstructures of AS_3 at $\theta \simeq 1.89^\circ$ with $P = 0$ and $\simeq$2.27 GPa is displayed in (e) and (f), respectively. The results of SM-$(AB)_2$ at $\theta \simeq 1.47^\circ$ with $P = 0$ and $\simeq$2.27 GPa are in (g) and (h), respectively.

when a vertical pressure is applied [85], thus increasing θ_{MA} as shown. Even though they could be quantitatively different, these tunable possibilities are commonly obtained in all TMGs as illustrated in figure 15 for AS_3 and SM-$(AB)_2$ structures.

Another tunability has been actually explored [4, 5, 8, 56, 57], i.e. by a vertical electric field (E-field) as illustrated in figures 16–18. First, figure 16 presents typical pictures showing the E-field effects in magic-angle twisted double bilayer graphene (i.e. DB-structure), compared to those in the TBLG structure. It shows that the E-field generally presents stronger effects in DB-structure than in TBLG one. This could be simply understood as a direct consequence of the fact that E-field can modulate the bandstructure and open

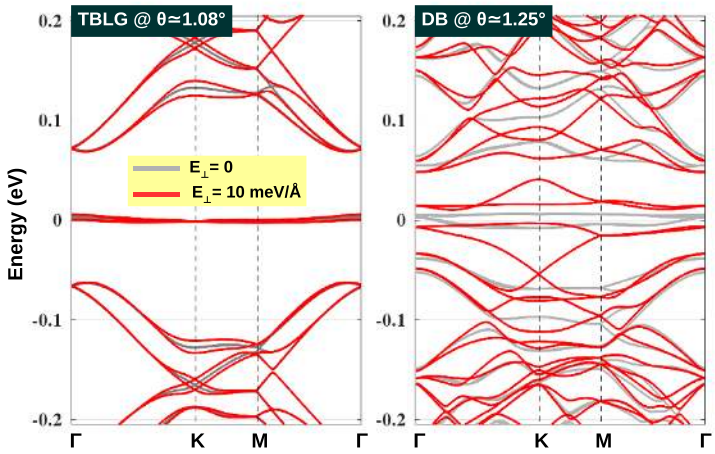

Figure 16. Effects of vertical electric field $E_\perp$ on the electronic bandstructure of TBLG at $\theta \simeq 1.08°$ and DM-structure at $\theta \simeq 1.25°$.

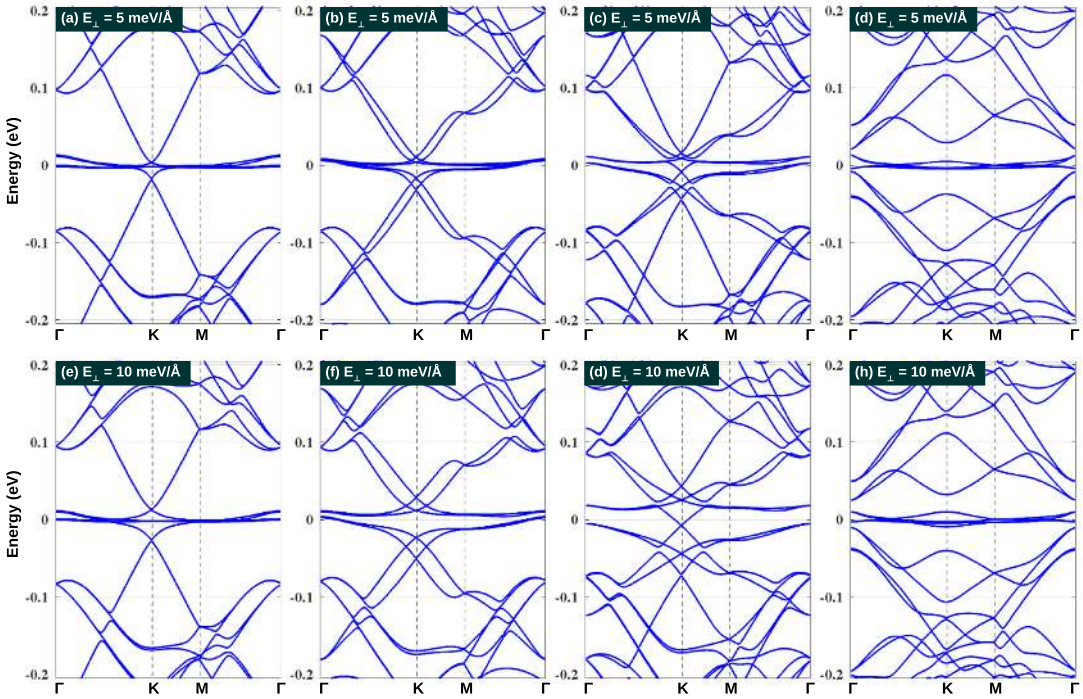

Figure 17. Electric field ($E_\perp$) effects on the electronic bandstructure of AS_3 at $\theta \simeq 1.54°$ (a) and (e), AS_4 at $\theta \simeq 1.70°$ (b) and (f), AS_5 at $\theta \simeq 1.79°$ (c) and (g), and AS_3 considered in figure 10(a) at $\theta \simeq 1.30°$ (d) and (h).

a bandgap in Bernal stacking bilayer graphene, which is not observed for monolayer graphene. These results thus emphasize that vertical E-field is a good degree of freedom to control the flat band and strongly correlated electronic phenomena in twisted systems containing Bernal stacking bilayer graphene, indeed as reported in [4, 5, 8, 56, 57].

Alternatively twisted multilayer systems of graphene monolayers (i.e. AS structures) is another example that has shown a good tunability by vertical E-field [6, 9, 11]. In particular, when an E-field is applied, a distinct feature observed in AS structures is that the flat bands can strongly hybridize with the Dirac bands, leading to the controllability of the bandwidth and interaction strength in the flat bands. In figure 17, the electronic bandstructure of AS_n ($n = 3, 4, 5$) is presented for two different E-fields. In addition to the mentioned hybridization, some other interesting effects are found. Indeed, while two flat bands hybridize with two Dirac bands, two other flat bands are still observed in the AS_3 case. For the AS_4 systems, four Dirac bands are observed at low energies (see figure 8) and hence the hybridization takes place for all four flat bands with these four Dirac bands when a large E-field is applied. Moreover, the hybridized flat bands can be

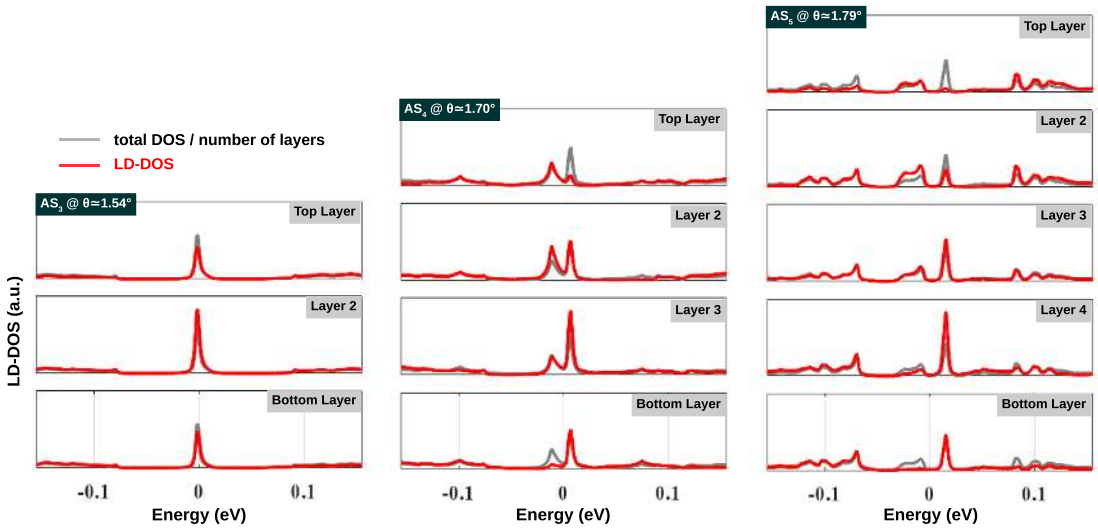

Figure 18. Layer decomposed DOS (LD-DOS) in systems considered in figures 17(e) and (f) when an electric field $E_\perp = 10$ meV Å^{-1} is applied.

separated in energy by the E-field. Similar features occur for AS_n systems with $n \geqslant 5$, except that besides four Dirac bands hybridizing with flat bands, the remaining Dirac bands are still observed near the Fermi level and a larger separation of hybridized flat bands is obtained.

For the AS_n structures investigated in figure 10 when a θ_{60} rotation is applied, the E-field even presents different effects, compared to the conventional cases in figure 8. In particular, instead of the band hybridization, flat bands in such systems are increasingly isolated from other dispersive bands when an E-field is applied, as seen in figures 17(d) and (h) for the AS_3 system of figure 10(a). These results could be simply understood by its different structural properties, compared to the conventional AS_3 one of figure 8 as analyzed in figure 11.

Finally, to clarify more completely those observed electronic features of AS_n systems, we analyze their layer decomposed DOS, when an E-field is applied, in figure 18. In the AS_3 case, even though the band hybridization occurs, changes in LD-DOS are relatively weak at the considered E-fields. This could be because besides two hybridized flat bands, other two flat bands are still preserved near the Fermi level as mentioned above. Stronger E-field effects on LD-DOS are found in the cases of a larger number of layers. In particular, the single localized DOS peak at zero E-field is generally separated into two peaks when an E-field is applied. Interestingly, those two peaks are shown to be likely separated in different layers. Indeed, the electron localized peak is mostly observed in the bottom layers whereas the hole peak in the top ones in the case of AS_4 and AS_5 systems in figure 18. These results suggest possibilities to control the spatial dependence of electron localization and therefore of strongly correlated electronic phenomena in those twisted systems.

6. Summary

Using atomistic calculations, the electronic properties of TMG systems are systematically studied. First, it is shown that both their structural and electronic properties exhibit a common feature that there is a unique magic angle at which the electronic localization in regions containing AA stacking configuration and its contribution to the global properties of the system are concurrently maximized. Flat electronic bands and strongly correlated electronic phenomena are therefore obtained at this critical case. In addition, the structural and electronic (particularly, electronic localization) properties are shown to exhibit a strong correlation. Consequently, the magic angle separates TMG systems into two classes, i.e. in small and large angle regimes, exhibiting distinct properties as clearly illustrated by the presented results obtained in TBLG [63]. Moreover, the strong correlation between the maximization of electronic localization in AA stacking region and the observation of flat bands presents an unknown physical view about the origin of magic angle. The electronic properties of magic-angle TMGs containing more than two graphene layers are shown to exhibit some other distinct properties, due to the presence of a large number of layers as well as various stacking configurations. In particular, the flat bands and dispersive ones at low energies can be concurrently obtained in some structures such as SM-$(AB)_n$ and alternatively twisted ones. The coexistence of localized-delocalized electronic states spatially separated are observed. At last, these TMGs present good

possibilities for tuning electronic properties by external fields. Finally, the magic angle is also shown to be nicely tunable by the effects of strain and/or vertical pressure. Our study thereby provides a comprehensive overview as well as highlights the essential and outstanding electronic properties of twisted graphene systems that could be helpful for further developments in *twistronics* research.

Data availability statement

All data that support the findings of this study are included within the article (and any supplementary files).

Acknowledgments

V H N and J-C C acknowledge financial support from the Fédération Wallonie-Bruxelles through the ARC Grants (Nos. 16/21-077 and 21/26-116), from the European Union's Horizon 2020 Research Project and Innovation Program—Graphene Flagship Core3 (No. 881603), from the Flag-Era JTC Project 'TATTOOS' (No. R.8010.19), from the EOS Project 'CONNECT' (No. 40007563) and from the Belgium F R S-FNRS through the research projects (Nos. T.0051.18 and T.029.22F). Computational resources have been provided by the CISM supercomputing facilities of UCLouvain and the CÉCI consortium funded by F R S-FNRS of Belgium (No. 2.5020.11). T X H acknowledges support from International Centre of Physics at the Institute of Physics, VAST, under Grant No. ICP.2022.05.

ORCID iD

V Hung Nguyen https://orcid.org/0000-0001-6729-3520

References

[1] Wu J-B, Zhang X, Ijäs M, Han W-P, Qiao X-F, Li X-Li, Jiang D-S, Ferrari A C and Tan P-H 2014 Resonant raman spectroscopy of twisted multilayer graphene *Nat. Commun.* **5** 5309
[2] Chen X-D, Xin W, Jiang W-S, Liu Z-B, Chen Y and Tian J-G 2016 High-precision twist-controlled bilayer and trilayer graphene *Adv. Mater.* **28** 2563–70
[3] Mogera U, Walia S, Bannur B, Gedda M and Kulkarni G U 2017 Intrinsic nature of graphene revealed in temperature-dependent transport of twisted multilayer graphene *J. Phys. Chem.* C **121** 13938–43
[4] Shen C *et al* 2020 Correlated states in twisted double bilayer graphene *Nat. Phys.* **16** 520–5
[5] Liu X *et al* 2020 Tunable spin-polarized correlated states in twisted double bilayer graphene *Nature* **583** 221–5
[6] Park J M, Cao Y, Watanabe K, Taniguchi T and Jarillo-Herrero P 2021 Tunable strongly coupled superconductivity in magic-angle twisted trilayer graphene *Nature* **590** 249–55
[7] Zhang Xi, Tsai K-T, Zhu Z, Ren W, Luo Y, Carr S, Luskin M, Kaxiras E and Wang K 2021 Correlated insulating states and transport signature of superconductivity in twisted trilayer graphene superlattices *Phys. Rev. Lett.* **127** 166802
[8] Chen S *et al* 2021 Electrically tunable correlated and topological states in twisted monolayer-bilayer graphene *Nat. Phys.* **17** 374–80
[9] Hao Z, Zimmerman A M, Ledwith P, Khalaf E, Najafabadi D H, Watanabe K, Taniguchi T, Vishwanath A and Kim P 2021 Electric field-tunable superconductivity in alternating-twist magic-angle trilayer graphene *Science* **371** 1133–8
[10] Brzhezinskaya M, Kononenko O, Matveev V, Zotov A, Khodos I I, Levashov V, Volkov V, Bozhko S I, Chekmazov S V and Roshchupkin D 2021 Engineering of numerous moire superlattices in twisted multilayer graphene for twistronics and straintronics applications *ACS Nano* **15** 12358–66
[11] Park J M, Cao Y, Xia L, Sun S, Watanabe K, Taniguchi T and Jarillo-Herrero P 2021 Magic-angle multilayer graphene: a robust family of moire superconductors (arXiv:2112.10760)
[12] Zhang S *et al* 2022 Domino-like stacking order switching in twisted monolayer-multilayer graphene *Nat. Mater.* (https://doi.org/10.1038/s41563-022-01232-2)
[13] Andrei E Y and MacDonald A H 2020 Graphene bilayers with a twist *Nat. Mater.* **19** 1265–75
[14] Wang J, Mu X, Wang L and Sun M 2019 Properties and applications of new superlattice: twisted bilayer graphene *Mater. Today Phys.* **9** 100099
[15] Carr S, Fang S and Kaxiras E 2020 Electronic-structure methods for twisted moiré layers *Nat. Rev. Mater.* **5** 748–63
[16] Bistritzer R and MacDonald A H 2011 Moiré bands in twisted double-layer graphene *Proc. Natl Acad. Sci.* **108** 12233–7
[17] Utama M I B *et al* 2021 Visualization of the flat electronic band in twisted bilayer graphene near the magic angle twist *Nat. Phys.* **17** 184–8
[18] Choi Y W and Choi H J 2018 Strong electron-phonon coupling, electron-hole asymmetry and nonadiabaticity in magic-angle twisted bilayer graphene *Phys. Rev.* B **98** 241412
[19] Kerelsky A *et al* 2019 Maximized electron interactions at the magic angle in twisted bilayer graphene *Nature* **572** 95–100
[20] Choi Y W and Choi H J 2021 Dichotomy of electron-phonon coupling in graphene moire flat bands *Phys. Rev. Lett.* **127** 167001
[21] Gadelha A C *et al* 2021 Localization of lattice dynamics in low-angle twisted bilayer graphene *Nature* **590** 405–9
[22] Gadelha A C, Nguyen V-H, Neto E G, Santana F, Raschke M B, Lamparski M, Meunier V, Charlier J-C and Jorio A 2021 Electron-phonon coupling in a magic-angle twisted-bilayer graphene device (arXiv:2110.14916)
[23] Barbosa T C, Gadelha A C, Ohlberg D A A, Watanabe K, Taniguchi T, Medeiros-Ribeiro G, Jorio A and Campos L C 2022 Raman spectra of twisted bilayer graphene close to the magic angle *2D Mater.* **9** 025007
[24] Cao Y, Fatemi V, Fang S, Watanabe K, Taniguchi T, Kaxiras E and Jarillo-Herrero P 2018 Unconventional superconductivity in magic-angle graphene superlattices *Nature* **556** 43–50
[25] Cao Y *et al* 2018 Correlated insulator behaviour at half-filling in magic-angle graphene superlattices *Nature* **556** 80–84

[26] Yankowitz M, Chen S, Polshyn H, Zhang Y, Watanabe K, Taniguchi T, Graf D, Young A F and Dean C R 2019 Tuning superconductivity in twisted bilayer graphene *Science* **363** 1059–64
[27] Xie Y, Lian B, Jäck B, Liu X, Chiu C-Li, Watanabe K, Taniguchi T, Bernevig B A and Yazdani A 2019 Spectroscopic signatures of many-body correlations in magic-angle twisted bilayer graphene *Nature* **572** 101–5
[28] Lu X *et al* 2019 Superconductors, orbital magnets and correlated states in magic-angle bilayer graphene *Nature* **574** 653–7
[29] Choi Y *et al* 2019 Electronic correlations in twisted bilayer graphene near the magic angle *Nat. Phys.* **15** 1174–80
[30] Jiang Y, Lai X, Watanabe K, Taniguchi T, Haule K, Mao J and Andrei E Y 2019 Charge order and broken rotational symmetry in magic-angle twisted bilayer graphene *Nature* **573** 91–95
[31] Sharpe A L, Fox E J, Barnard A W, Finney J, Watanabe K, Taniguchi T, Kastner M A and Goldhaber-Gordon D 2019 Emergent ferromagnetism near three-quarters filling in twisted bilayer graphene *Science* **365** 605–8
[32] Serlin M, Tschirhart C L, Polshyn H, Zhang Y, Zhu J, Watanabe K, Taniguchi T, Balents L and Young A F 2020 Intrinsic quantized anomalous Hall effect in a moire heterostructure *Science* **367** 900–3
[33] Balents L, Dean C R, Efetov D K and Young A F 2020 Superconductivity and strong correlations in moiré flat bands *Nat. Phys.* **16** 725–33
[34] Carr S, Massatt D, Fang S, Cazeaux P, Luskin M and Kaxiras E 2017 Twistronics: manipulating the electronic properties of two-dimensional layered structures through their twist angle *Phys. Rev.* B **95** 075420
[35] Liu K, Zhang L, Cao T, Jin C, Qiu D, Zhou Q, Zettl A, Yang P, Louie S G and Wang F 2014 Evolution of interlayer coupling in twisted molybdenum disulfide bilayers *Nat. Commun.* **5** 4966
[36] Kang P, Zhang W-T, Michaud-Rioux V, Kong X-H, Hu C, Yu G-H and Guo H 2017 Moiré impurities in twisted bilayer black phosphorus: effects on the carrier mobility *Phys. Rev.* B **96** 195406
[37] Naik M H and Jain M 2018 Ultraflatbands and shear solitons in moire patterns of twisted bilayer transition metal dichalcogenides *Phys. Rev. Lett.* **121** 266401
[38] Xian L, Kennes D M, Tancogne-Dejean N, Altarelli M and Rubio A 2019 Multiflat bands and strong correlations in twisted bilayer boron nitride: doping-induced correlated insulator and superconductor *Nano Lett.* **19** 4934–40
[39] Yang Y, Li J, Yin J, Xu S, Mullan C, Taniguchi T, Watanabe K, Geim A K, Novoselov K S and Mishchenko A 2020 *In situ* manipulation of van der Waals heterostructures for twistronics *Sci. Adv.* **6** eabd3655
[40] Kennes D M, Claassen M, Xian L, Georges A, Millis A J, Hone J, Dean C R, Basov D N, Pasupathy A N and Rubio A 2021 Moire heterostructures as a condensed-matter quantum simulator *Nat. Phys.* **17** 155–63
[41] Xu Q, Guo Y and Xian L 2021 Moiré flat bands in twisted 2D hexagonal vdW materials *2D Mater.* **9** 014005
[42] Tao S, Zhang X, Zhu J, He P, Yang S A, Lu Y and Wei S-H 2022 Designing ultra-flat bands in twisted bilayer materials at large twist angles: theory and application to two-dimensional indium selenide *J. Am. Chem. Soc.* **144** 3949–56
[43] Liu M, Wang L and Yu G 2022 Developing graphene-based moire heterostructures for twistronics *Adv. Sci.* **9** 2103170
[44] Tong Q, Liu F, Xiao J and Yao W 2018 Skyrmions in the moire of van der Waals 2D magnets *Nano Lett.* **18** 7194–9
[45] Wang C, Gao Y, Lv H, Xu X and Xiao Di 2020 Stacking domain wall magnons in twisted van der Waals magnets *Phys. Rev. Lett.* **125** 247201
[46] Song T *et al* 2021 Direct visualization of magnetic domains and moire magnetism in twisted 2D magnets *Science* **374** 1140–4
[47] Luo Xi-W and Zhang C 2021 Spin-twisted optical lattices: tunable flat bands and Larkin-Ovchinnikov superfluids *Phys. Rev. Lett.* **126** 103201
[48] Jin Z *et al* 2022 Controlled synthesis of a two-dimensional non-van der Waals ferromagnet toward a magnetic moiré superlattice *ACS Nano* (https://doi.org/10.1021/acsnano.1c11018)
[49] Wang W, Gao W, Chen X, Shi F, Li G, Dong J, Xiang Y and Zhang S 2020 Moire fringe induced gauge field in photonics *Phys. Rev. Lett.* **125** 203901
[50] Mao X-R, Shao Z-K, Luan H-Y, Wang S-L and Ma R-M 2021 Magic-angle lasers in nanostructured moire superlattice *Nat. Nanotechnol.* **16** 1099–105
[51] Zhang Q, Hu G, Ma W, Li P, Krasnok A, Hillenbrand R, Alu A and Qiu C-W 2021 Interface nano-optics with van der Waals polaritons *Nature* **597** 187–95
[52] Chen J, Lin X, Chen M, Low T, Chen H and Dai S 2021 A perspective of twisted photonic structures *Appl. Phys. Lett.* **119** 240501
[53] Khalaf E, Kruchkov A J, Tarnopolsky G and Vishwanath A 2019 Magic angle hierarchy in twisted graphene multilayers *Phys. Rev.* B **100** 085109
[54] Haddadi F, Wu Q, Kruchkov A J and Yazyev O V 2020 Moiré flat bands in twisted double bilayer graphene *Nano Lett.* **20** 2410–5
[55] Park Y, Chittari B L and Jung J 2020 Gate-tunable topological flat bands in twisted monolayer-bilayer graphene *Phys. Rev.* B **102** 035411
[56] Choi Y W and Choi H J 2019 Intrinsic band gap and electrically tunable flat bands in twisted double bilayer graphene *Phys. Rev.* B **100** 201402
[57] Rickhaus P *et al* 2021 Correlated electron-hole state in twisted double-bilayer graphene *Science* **373** 1257–60
[58] Tritsaris G A, Carr S, Zhu Z, Xie Y, Torrisi S B, Tang J, Mattheakis M, Larson D T and Kaxiras E 2020 Electronic structure calculations of twisted multi-layer graphene superlattices *2D Mater.* **7** 035028
[59] Carr S, Fang S, Zhu Z and Kaxiras E 2019 Exact continuum model for low-energy electronic states of twisted bilayer graphene *Phys. Rev. Res.* **1** 013001
[60] Tritsaris G A, Carr S, Zhu Z, Xie Y, Torrisi S B, Tang J, Mattheakis M, Larson D T and Kaxiras E 2020 Electronic structure calculations of twisted multi-layer graphene superlattices *2D Mater.* **7** 035028
[61] Shin J, Chittari B L and Jung J 2021 Stacking and gate-tunable topological flat bands, gaps and anisotropic strip patterns in twisted trilayer graphene *Phys. Rev.* B **104** 045413
[62] Gargiulo F and Yazyev O V 2017 Structural and electronic transformation in low-angle twisted bilayer graphene *2D Mater.* **5** 015019
[63] Hung Nguyen V, Paszko D, Lamparski M, van Troeye B, Meunier V and Charlier J-C 2021 Electronic localization in small-angle twisted bilayer graphene *2D Mater.* **8** 035046
[64] Lindsay L and Broido D A 2010 Optimized Tersoff and Brenner empirical potential parameters for lattice dynamics and phonon thermal transport in carbon nanotubes and graphene *Phys. Rev.* B **81** 205441
[65] Kolmogorov A N and Crespi V H 2005 Registry-dependent interlayer potential for graphitic systems *Phys. Rev.* B **71** 235415
[66] Leven I, Maaravi T, Azuri I, Kronik L and Hod O 2016 Interlayer potential for graphene/*h*-BN heterostructures *J. Chem. Theory Comput.* **12** 2896–905

[67] Brihuega I, Mallet P, González-Herrero H, de Laissardière G T, Ugeda M M, Magaud L, Gómez-Rodríguez J M, Ynduráin F and Veuillen J-Y 2012 Unraveling the intrinsic and robust nature of van Hove singularities in twisted bilayer graphene by scanning tunneling microscopy and theoretical analysis *Phys. Rev. Lett.* **109** 196802
[68] Yoo H *et al* 2019 Atomic and electronic reconstruction at the van der Waals interface in twisted bilayer graphene *Nat. Mater.* **18** 448–53
[69] Zhang S *et al* 2020 Abnormal conductivity in low-angle twisted bilayer graphene *Sci. Adv.* **6** eabc5555
[70] Uchida K, Furuya S, Iwata J-I and Oshiyama A 2014 Atomic corrugation and electron localization due to moire patterns in twisted bilayer graphenes *Phys. Rev.* B **90** 155451
[71] Cantele G, Alfè D, Conte F, Cataudella V, Ninno D and Lucignano P 2020 Structural relaxation and low-energy properties of twisted bilayer graphene *Phys. Rev. Res.* **2** 043127
[72] Lamparski M, Van Troeye B and Meunier V 2020 Soliton signature in the phonon spectrum of twisted bilayer graphene *2D Mater.* **7** 025050
[73] de Laissardière G T, Mayou D and Magaud L 2012 Numerical studies of confined states in rotated bilayers of graphene *Phys. Rev.* B **86** 125413
[74] Yin L-J, Qiao J-B, Wang W-X, Zuo W-J, Yan W, Xu R, Dou R-F, Nie J-C and He L 2015 Landau quantization and Fermi velocity renormalization in twisted graphene bilayers *Phys. Rev.* B **92** 201408
[75] Tong L-H, Tong Q, Yang Li-Z, Zhou Y-Y, Wu Q, Tian Y, Zhang Li, Zhang L, Qin Z and Yin L-J 2022 Spectroscopic visualization of flat bands in magic-angle twisted monolayer-bilayer graphene: coexistence of localization and delocalization *Phys. Rev. Lett.* **128** 126401
[76] Zhang C *et al* 2021 Visualizing delocalized correlated electronic states in twisted double bilayer graphene *Nat. Commun.* **12** 2516
[77] Koshino M 2010 Interlayer screening effect in graphene multilayers with *ABA* and *ABC* stacking *Phys. Rev.* B **81** 125304
[78] Wu Z, Kuang X, Zhan Z and Yuan S 2021 Magic angle and plasmon mode engineering in twisted trilayer graphene with pressure *Phys. Rev.* B **104** 205104
[79] Finney N R, Yankowitz M, Muraleetharan L, Watanabe K, Taniguchi T, Dean C R and Hone J 2019 Tunable crystal symmetry in graphene-boron nitride heterostructures with coexisting moiré superlattices *Nat. Nanotechnol.* **14** 1029–34
[80] Hung Nguyen V and Dollfus P 2015 Strain-induced modulation of Dirac cones and van Hove singularities in a twisted graphene bilayer *2D Mater.* **2** 035005
[81] Huder L, Artaud A, Le Quang T, de Laissardière G T, Jansen A G M, Lapertot G, Chapelier C and Renard V T 2018 Electronic spectrum of twisted graphene layers under heterostrain *Phys. Rev. Lett.* **120** 156405
[82] Lin X, Zhu H and Ni J 2020 Pressure-induced gap modulation and topological transitions in twisted bilayer and twisted double bilayer graphene *Phys. Rev.* B **101** 155405
[83] Liu Y-W *et al* 2020 Tunable lattice reconstruction, triangular network of chiral one-dimensional states and bandwidth of flat bands in magic angle twisted bilayer graphene *Phys. Rev. Lett.* **125** 236102
[84] Szentpéteri B *et al* 2021 Tailoring the band structure of twisted double bilayer graphene with pressure *Nano Lett.* **21** 8777–84
[85] To model the effects of vertical pressure P, the average interlayer distance d is fixed and modified (in relaxation simulations) with respect to its equilibrium value d_0. The same approach is applied to superlattice vectors to model in-plane strains. P is estimated as in Phys. Rev. B 98, 085144 (2018), i.e. $P = A(e^{-B\epsilon} - 1)$ with $A = 5.73$ GPa, $B = 9.54$, and $\epsilon = 1 - (d/d_0)$